

Improving the full spectrum fitting method: accurate convolution with Gauss-Hermite functions

Michele Cappellari^{*}

Sub-Department of Astrophysics, Department of Physics, University of Oxford, Denys Wilkinson Building, Keble Road, Oxford, OX1 3RH

Submitted to MNRAS on 28 July 2016

ABSTRACT

I start by providing an updated summary of the penalized pixel-fitting (PPXF) method, which is used to extract the stellar and gas kinematics, as well as the stellar population of galaxies, via full spectrum fitting. I then focus on the problem of extracting the kinematics when the velocity dispersion σ is smaller than the velocity sampling Δv , which is generally close to the instrumental resolution σ_{inst} , by design. The same situation arises when measuring line-of-sight velocities of individual stars. The standard approach is mathematically equivalent to convolving with a discretized kernel, via direct summation, while fitting for the kernel parameters. However, this approach obviously becomes seriously inaccurate when $\sigma \lesssim \Delta v/2$, due to undersampling. Oversampling can be used to prevent this, but it has drawbacks. Here I present a better alternative, which is not only more accurate and efficient, but even simpler to implement. It consists of avoiding the evaluation of the under-sampled kernel, and instead directly computing its well-sampled analytic Fourier transform, for use with the convolution theorem. A simple analytic transform exists when the kernel is described by the standard Gauss-Hermite parametrization (of which the Gaussian is a special case) for the line-of-sight velocity distribution. I describe how this idea was implemented in a significant upgrade to the publicly available PPXF software. As expected, the proposed approach recovers accurate kinematics irrespective of σ . Gaussian convolution algorithms used in today’s popular software packages also suffer from undersampling, when σ is smaller than the pixel size. They could all be easily fixed as proposed here.

Key words: techniques: radial velocities – techniques: spectroscopic – galaxies: kinematics and dynamics

1 INTRODUCTION

The kinematics of the stars and gas in galaxies is a key ingredient in our understanding of how they form and evolve. Nowadays, this information is extracted from integral-field spectroscopic (IFS) data, which provide a three dimensional view of galaxies. The technology is now available on all major telescopes and is quickly becoming the standard way of obtaining spectra for galaxy evolution studies (see Cappellari 2016, for a review).

The IFS data provide a “fossil record” of galaxy formation. Specifically, the IFS kinematics of the stars allow one to distinguish a galaxy assembly dominated by gas poor merging from a growth driven by gas accretion and star formation (e.g. Emsellem et al. 2011; Cappellari et al. 2013b; Naab et al. 2014). Dynamical models based on IFS kinematics allow one to infer the galaxies mass distributions to study scaling relations (e.g. Cappellari et al. 2013a; Scott et al. 2015), the stellar and dark matter content (e.g. Cappellari et al. 2012, 2015), or measure black hole masses (e.g. Krajnović et al. 2009; Seth et al. 2014; Walsh et al. 2016). While

the gas content and kinematics tell us about the role of gas accretion in galaxy assembly (e.g. Sarzi et al. 2006; Davis et al. 2011; Barrera-Ballesteros et al. 2015) or the mechanism that regulates star formation in galaxies (e.g. Alatalo et al. 2011; Cheung et al. 2016; Ho et al. 2016).

For more than a decade, this information has been extracted from IFS data by surveys targeting one galaxy at a time (SAURON de Zeeuw et al. 2002; DiskMass Bershadsky et al. 2010; ATLAS^{3D} Cappellari et al. 2011; CALIFA Sánchez et al. 2012). But the observational panorama is undergoing a revolution, with the arrival of large multiplexed IFS surveys targeting 10–20 galaxies at a time. Thousands of galaxies have already been observed in this manner (MaNGA Bundy et al. 2015; SAMI Bryant et al. 2015).

These ongoing IFS surveys depend critically on the full spectrum fitting technique to deliver their science. The method is used to extract stellar and gas kinematics, as well as stellar population from the spectral data cubes. But, given the large number of objects and the variety of galaxy morphological types, these surveys are pushing the existing techniques to their limits.

This paper is motivated by the existence of these ongoing large surveys and mostly arises from initial experiences with the analy-

^{*} E-mail: michele.cappellari@physics.ox.ac.uk

sis of the MaNGA data. I realized that all the spectrum fitting approaches, which are nearly universally adopted to extract stellar and gas kinematics, can be significantly improved. Here in [section 2](#) I describe general concepts about kinematic extraction, in [section 3](#) I give an updated summary of the PPXF method, in [section 4](#) I discuss problems of the current approach and propose a clean solution, I summarize my paper in [section 5](#).

2 GENERAL CONCEPTS

For external galaxies, or other stellar systems not resolved into individual stars, the stellar kinematics information is extracted by comparing the observed spectra, at different spatial locations, with broadened stellar templates. This comparison is nowadays almost invariably performed in pixel space rather than in Fourier space (e.g. [Rix & White 1992](#); [van der Marel 1994](#); [Kelson et al. 2000](#); [Cappellari & Emsellem 2004](#)). This is because it makes the masking of bad pixels, or the simultaneous extraction of gas kinematics and stellar population, an easy and accurate process, while also allowing for other observational effects to be easily modelled.

In this section I review some general concepts, useful for understanding the how kinematics is generally extracted from galaxy spectra. I also try to clarify aspect that I discovered can lead to potential mistakes, from more than a decade of feedback I received from users of my publicly-available Penalized Pixel-Fitting software PPXF ([Cappellari & Emsellem 2004](#)).

2.1 Templates observed like the galaxy spectrum

More than a decade ago, the stellar templates were generally observed with the same spectrograph used to obtain the galaxy spectrum under analysis (e.g. [van der Marel et al. 1994](#)). In this way one could assume that all the difference between the galaxy spectrum and the templates was due to the broadening by the galaxy line-of-sight velocity distribution (LOSVD). In this idealized case one could schematically model the galaxy spectrum G_{mod} as follows

$$G_{\text{mod}}(x) = T(x) * \mathcal{L}(cx), \quad (1)$$

where $x = \ln \lambda$ is the natural logarithm of wavelength, $T(x)$ is the stellar template, \mathcal{L} is the LOSVD, with c the speed of light and $*$ denoting convolution.

It is worth noting that the use of a logarithmic axis, although universally adopted in the past few decades, is not strictly required for the kinematic extraction. It ensures a constant velocity scale for every x . This means that $\mathcal{L}(v)$ remains constant along the x coordinate and allows one to use efficient Fast Fourier Transform (FFT) methods when performing the convolution.

In principle however, it would also be possible to perform the convolution in linear λ . For this one would need to allow for the $\mathcal{L}(v)$ to vary with x , but one could still construct a relatively efficient convolution, via direct summation, by making use of the fact that the convolution kernel $\mathcal{L}(v)$ generally consists of a few orders of magnitude fewer elements than the galaxy and templates spectra. However, given that at least one resampling is unavoidable when reducing the spectral data, there are currently no compelling reasons to stop using logarithmic coordinates.

2.2 Templates from spectral libraries

In the past decade, thanks to the availability of high resolution empirical stellar libraries spanning large ranges of atmospheric pa-

rameters over a wide wavelength range (e.g. [Cenarro et al. 2001](#); [Sánchez-Blázquez et al. 2006](#); [Prugniel & Soubiran 2001](#)), libraries of synthetic stellar spectra (e.g. [Munari et al. 2005](#); [Gustafsson et al. 2008](#)), and stellar population models based on these libraries (e.g. [Bruzual & Charlot 2003](#); [Vazdekis et al. 2010](#); [Maraston & Strömbäck 2011](#); [Conroy & van Dokkum 2012](#)), it has become common practice to extract the stellar kinematics by employing as templates linear combinations of a large number (up to a thousand) of stellar templates observed with a different spectrograph than the one used to obtain the galaxy spectra.

Due to this difference, before the kinematic extraction, and assuming the templates have a better resolution than the galaxy spectrum, the templates need to be matched to the galaxy spectrum by convolving them with a kernel $K(x, \lambda)$, which generally varies with wavelength λ , defined by the relation

$$\text{LSF}_{\text{inst}}(x, \lambda) = \text{LSF}_{\text{temp}}(x, \lambda) * K(x, \lambda). \quad (2)$$

Here $\text{LSF}_{\text{inst}}(x, \lambda)$ is the galaxy line-spread function, which describes the observed shape of an intrinsically very narrow spectral line (in principle a δ function) at the wavelength λ , due to purely instrumental broadening. $\text{LSF}_{\text{temp}}(x, \lambda)$ is the LSF for the templates. After the templates have been convolved as

$$\tilde{T}(x) = T(x) * K(x, \lambda), \quad (3)$$

they become as if they had been observed with the same spectrograph as the galaxy, and one can still model the galaxy spectrum with [equation \(1\)](#). Note that [equation \(3\)](#) is not a standard convolution, due to the λ dependence in the kernel. In signal processing this is called general convolution or general superposition integral.

In principle the kernel $K(x, \lambda)$ could be measured in the very same way one uses to extract the LOSVD, e.g. using spectra of the twilight sky. However, in practice, it is quite difficult to accurately characterize the spectral, spatial and temporal variation of the $\text{LSF}_{\text{inst}}(x, \lambda)$ and $\text{LSF}_{\text{temp}}(x, \lambda)$ in the data. Moreover, the LSFs turn out to be generally well represented by Gaussian functions.

It is well known that the convolution of two normalized Gaussians with dispersion σ_a and σ_b is another normalized Gaussian with dispersion $\sigma_c^2 = \sigma_a^2 + \sigma_b^2$ (e.g. [Brigham 1974](#), §2). For these reasons, when the LSF are assumed Gaussian, instead of applying [equation \(3\)](#), one convolves the templates with a normalized Gaussian

$$G_{\text{diff}}(x, \lambda) = \frac{\exp\{-x^2/[2\sigma_{\text{diff}}^2(\lambda)]\}}{\sigma_{\text{diff}}(\lambda)\sqrt{2\pi}} \quad (4)$$

with dispersion

$$\sigma_{\text{diff}}^2(\lambda) = \sigma_{\text{inst}}^2(\lambda) - \sigma_{\text{temp}}^2(\lambda), \quad (5)$$

where σ_{inst} and σ_{temp} are the Gaussian dispersion of the LSF for the instrument used to observe the galaxy and for the one used to obtain the stellar templates, respectively.

Given the λ dependence of σ_{diff} , the general convolution in [equation \(3\)](#) needs to be performed via direct summation rather than using FFTs. But this only need to be done once, before fitting the LOSVD and for this reason its computation is not time critical. However, special care needs to be taken to avoid under-sampling during the computation of [equation \(3\)](#), as it can be affected by the same under-sampling issues discussed in [subsection 4.2](#).

2.3 From measured velocity to observed redshift

One important aspect that often causes confusion to users of spectral fitting software, is the connection between the measured line-

of-sight velocity V and the galaxy redshift z . For this reason I clarify this aspect here.

As described in [subsection 2.1](#), spectral fitting codes rebin the spectra logarithmically and measure velocities from the shift Δx required to match the spectral templates to the galaxy spectrum. This shift is precisely related to the redshift as follows

$$\Delta x = \Delta \ln \lambda = \ln(\lambda_{\text{obsv}}/\lambda_{\text{emit}}) = \ln(1 + z). \quad (6)$$

However, spectral fitting codes also need to define a velocity scale to be used as variable in the LOSVD (e.g. to quantify the galaxy velocity dispersion). For small velocity differences ΔV , the Doppler formula is

$$\Delta V \approx c \frac{\Delta \lambda}{\lambda_{\text{emit}}} \approx c \Delta \ln \lambda. \quad (7)$$

So one can *define* a constant velocity scale per pixel, which reduces to the Doppler formula in the limit of small ΔV , namely on the scale of the LOSVD

$$V \equiv c \Delta x = c \Delta \ln \lambda = c \ln(1 + z). \quad (8)$$

This definition is used to convert the pixels differences Δx measured by the codes into velocities, to provide the V and σ in km s^{-1} . Given this definition, one has to use [equation \(8\)](#) to convert back the measured velocities into redshifts, when needed. In particular, the well known approximation $z \approx V/c$ should *never* be used, being already less accurate than the typical measurement uncertainties when $z \gtrsim 0.01$.

2.4 Separating peculiar velocities and cosmological redshift

In the common case of IFS data, one is interested in the stellar and gas velocities V_{bin} measured within different spatial bins within a galaxy (e.g. to construct dynamical models, or measure gas outflows) and not in the actual redshift z_{bin} of the individual spectra. When the redshift is negligible ($z \lesssim 0.01$), the V_{bin} can be computed with sufficient accuracy by simply subtracting the velocity V_{sys} of the galaxy barycentre from the measured velocities V directly provided by the spectral fitting program. However this simple approach will lead to *dramatic* errors at larger redshift, where a quite different approach must be used.

In cosmology, the V_{bin} are called ‘peculiar velocities’, to distinguish them from the cosmological recession velocity or redshift z_{cosm} . The latter is formally defined as the redshift of the galaxy barycentre. For galaxies at significant redshift, a simple approach to measure V_{bin} consists of bringing all the galaxy spectra onto the rest frame by dividing their wavelength by $(1 + z'_{\text{cosm}})$, where z'_{cosm} is an initial estimate of the galaxy redshift. This division is actually equivalent to merely re-defining the origin of the velocity coordinate, while keeping the spectra unchanged. Crucially, the galaxy $\text{LSF}_{\text{inst}}(x, \lambda)$ must be compressed by the same factor or, when this is assumed Gaussian, its σ_{inst} (in λ units) must also be divided by $(1 + z'_{\text{cosm}})$.

Once these two steps have been performed, the velocities V returned by the spectral fitting program will be the desired V_{bin} . From the extracted rest-frame velocity field, one can accurately measure possible residual offsets V_{bary} of the barycentre velocity from zero, by enforcing symmetries in the field (e.g. [Krajnović et al. 2006](#), appendix C). This *small* offset can just be subtracted from all V_{bin} . Finally, an improved estimate of the galaxy redshift can be obtained using the relation (e.g. [Cappellari et al. 2009](#), eq. 2)

$$1 + z_{\text{cosm}} = (1 + z'_{\text{cosm}}) \times (1 + V_{\text{bary}}/c). \quad (9)$$

which derives from the general expression linking the cosmological redshift z_{cosm} , the bins peculiar velocities V_{bin} and the observed bins redshift z_{bin} (e.g. [Hogg 1999](#), eq. 10)

$$1 + z_{\text{bin}} = (1 + z_{\text{cosm}}) \times (1 + V_{\text{bin}}/c). \quad (10)$$

3 OVERVIEW OF THE PPXF METHOD

One particular technique used to extract stellar kinematics is called the Penalized Pixel Fitting (PPXF) method. It was originally described in [Cappellari & Emsellem \(2004\)](#), but it has significantly evolved over more than a decade of intense usage, to address our own specific needs and requests or feedback from users. A number of the new features in PPXF were not described in detail the literature and for this reason are summarized in this section. I describe here the current version 6.0 of the Python implementation of the software¹. But most of the features are also implemented in the IDL version of PPXF.

3.1 Model for the galaxy spectrum

The method approximates the observed galaxy spectrum via the following quite general parametrization:

$$G_{\text{mod}}(x) = \sum_{n=1}^N w_n \left\{ [T_n(x) * \mathcal{L}_n(cx)] \sum_{k=1}^K a_k \mathcal{P}_k(x) \right\} + \sum_{l=0}^L b_l \mathcal{P}_l(x) + \sum_{j=1}^J c_j S_j(x), \quad (11)$$

where the \mathcal{L}_n are the LOSVDs, which can be different for the N templates T_n (e.g. [Johnston et al. 2013](#)), the \mathcal{P}_k and \mathcal{P}_l are multiplicative or additive orthogonal polynomials respectively (of Legendre type or a truncated Fourier series), and S_j are spectra of the sky (e.g. [Weijmans et al. 2009](#)). Optionally, the multiplicative polynomial can be replaced with the expression

$$f(x) = 10^{-0.4 E(B-V) k(x)} \quad (12)$$

where $k(x)$ is a reddening curve (e.g. [Cardelli et al. 1989](#); [Calzetti et al. 2000](#)) and $E(B-V)$ quantifies the amount of reddening, which is constrained to be positive. Any of the polynomials or sky components is optional and does not need to be actually used during a PPXF fit.

There is considerable freedom in the choice of templates depending on the specific application. The templates can consist of combinations of e.g. (i) individual empirical (e.g. [Cenarro et al. 2001](#); [Sánchez-Blázquez et al. 2006](#); [Prugniel & Soubiran 2001](#)) or synthetic (e.g. [Munari et al. 2005](#); [Gustafsson et al. 2008](#)) stars, (ii) stellar population models with specific parameters (e.g. [Bruzual & Charlot 2003](#); [Vazdekis et al. 2010](#); [Maraston & Strömbäck 2011](#); [Conroy & van Dokkum 2012](#)), (iii) principal components derived from a library of spectra, (iv) weighted sum of different stars, (v) gas emission lines or (vi) sky spectra. The first choice is generally preferred when extracting stellar kinematics (e.g. [Cappellari et al. 2011](#)), due to the extra freedom to fit spectra in detail, while the second option is used when PPXF is employed for ‘full spectrum’ fitting to study the galaxies stellar population (e.g. [Onodera et al. 2012](#); [Cappellari et al. 2012](#); [McDermid et al. 2015](#); [Morelli et al. 2015](#); [Shetty & Cappellari 2015](#)).

¹ Available from <http://purl.org/cappellari/software>

3.2 Parametrization for the LOSVD

The LOSVD $\mathcal{L}_n(v)$, for both the stellar and gas templates, are parametrized using the Gauss-Hermite parametrization introduced for this purpose by [van der Marel & Franx \(1993\)](#) and [Gerhard \(1993\)](#). However, it is important to emphasize that the two papers did not quite define the same parametrization for the LOSVD. The crucial difference is that, while [Gerhard \(1993\)](#) fitted all moments in the Gauss-Hermite expansion, [van der Marel & Franx \(1993\)](#) chose to explicitly set the first three coefficients to $(h_0, h_1, h_2) = (1, 0, 0)$, and only fit the higher coefficients, in such a way that the LOSVD has the form

$$\mathcal{L}(y) = \frac{\exp(-y^2/2)}{\sigma \sqrt{2\pi}} \left[1 + \sum_{m=3}^M h_m H_m(y) \right], \quad (13)$$

$$y = (v - V)/\sigma$$

It was the latter form, of [equation \(13\)](#), which has become the current standard in the field (e.g. [Bender et al. 1994](#)) and was also adopted by PPXF. Here, H_m are the Hermite polynomials, standardized (by definition) in such a way that the terms of [equation \(13\)](#) are solutions of the one-dimensional quantum harmonic oscillator (e.g. [Schiff 1968](#), §4)

$$H_m(y) = \frac{H_i(y)}{\sqrt{i! 2^i}}, \quad (14)$$

were the H_i are the so-called ‘physicists’ Hermite polynomials, defined as in [equation \(22.2.14\)](#) of [Abramowitz & Stegun \(1964\)](#). The H_i polynomials are the ones most commonly provided by default by today’s popular software. They are e.g. the form returned by MATHEMATICA’s function `HermiteH`, or by NUMPY’s `polynomial.hermite.hermval`, or by MATLAB’s function `hermiteH`. The first five Hermite polynomials H_m are given e.g. in [equation \(A5\)](#) of [van der Marel & Franx \(1993\)](#).

3.3 Linear fitting procedure

For every choice of the non-linear parameters in the model of [equation \(11\)](#)

$$(V, \sigma, h_3, \dots, h_M, a_1, \dots, a_K), \quad (15)$$

PPXF minimizes the functional (e.g. [Press et al. 2007](#), §19.5)

$$\mathcal{F} = \chi^2 + \lambda \mathcal{B} \quad (16)$$

where the first term measures the agreement between the model spectrum G_{mod} and the observed galaxy spectrum G , while the second is an adjustable term, which can be zero, and which quantifies the smoothness of the weights, in a space spanned by the population parameters (e.g. age, metallicity and α enhancement).

In the general case in which one knows the covariance matrix Σ of the spectral pixels, the agreement between data and model is quantified by

$$\begin{aligned} \chi^2 &= [\mathbf{A} \cdot \mathbf{x} - \mathbf{y}]^T \cdot \Sigma^{-1} \cdot [\mathbf{A} \cdot \mathbf{x} - \mathbf{y}] \\ &= |(\mathbf{L}^{-1} \cdot \mathbf{A}) \cdot \mathbf{x} - \mathbf{L}^{-1} \cdot \mathbf{y}|^2 = |\mathbf{r}|^2, \end{aligned} \quad (17)$$

where the columns of the matrix \mathbf{A} consist of the convolved templates (multiplied by the polynomials), the additive polynomials and the sky spectra, \mathbf{r} is the vector of residuals, the vector

$$\mathbf{x} = (w_1, \dots, w_N, b_0, \dots, b_L, c_1, \dots, c_J), \quad (18)$$

with $w_n \geq 0$ and $c_j \geq 0$

and $\Sigma = \mathbf{L} \cdot \mathbf{L}^T$ is the Cholesky decomposition (e.g. [Press et al. 2007](#), §2.9) of the positive-definite covariance matrix.

The minimization of the χ^2 in [equation \(17\)](#) is a quadratic programming problem. It is solved in PPXF by finding the least-squares solution, with positivity constraints on some variables, of the linear system

$$(\mathbf{L}^{-1} \cdot \mathbf{A}) \cdot \mathbf{x} = \mathbf{L}^{-1} \cdot \mathbf{y}. \quad (19)$$

Specific and efficient algorithms exist to solve this type of problems, with guaranteed convergence in a finite number of steps to the global minimum. Currently the IDL version of PPXF uses the Bounded-Variables Least Squares (BVLS) algorithm by [Lawson & Hanson \(1974\)](#), while the Python version uses the Non-Negative Least Squares (NNLS) code by the same authors, made available by Scipy’s `optimize.nnls`, while employing slack variables to remove the positivity constraints from the additive polynomials coefficients (b_0, \dots, b_L) .

In the common situation where spectral covariance is ignored and one only knows the error spectrum, then \mathbf{L}^{-1} reduces to a diagonal matrix with diagonal elements $1/\Delta G(x_p)$, where $\Delta G(x_p)$ is the 1σ uncertainty of every pixel x_i in the galaxy spectrum. In this special, but usual case the residual vector has elements

$$r_p = \frac{G_{\text{mod}}(x_p) - G(x_p)}{\Delta G(x_p)}. \quad (20)$$

3.4 Non-linear fitting procedure

A key feature of PPXF, from which the method derives its name, is the fact that it automatically penalizes non-Gaussian solutions, to reduce the noise in the recovered kinematics, when the data do not contain sufficient information to constrain the shape of the LOSVD. This is done by minimizing a new objective function

$$\chi_p^2 = \chi^2 + \alpha \mathcal{P}, \quad (21)$$

where the χ^2 is given in [equation \(17\)](#) or [equation \(20\)](#), \mathcal{P} is a penalty function, which describes the deviation of the LOSVD from a Gaussian shape, while α is an adjustable penalty, which depends on the data quality. The penalty is implemented in an efficient way, by perturbing the residual vector \mathbf{r} in such a way that the sum-of-squares nature of the problem is preserved. This is described in the original paper ([Cappellari & Emsellem 2004](#), section 3.3) and will not be repeated here.

In both cases, with or without the covariance matrix, the minimization of the χ_p^2 as a function of the non-linear parameters in [equation \(15\)](#) is performed with the specific Levenberg-Marquardt non-linear least-squares optimization algorithm (e.g. [Press et al. 2007](#), §15.5.2). This makes use of the sum-of-squares nature of the optimization problem by requiring the user to provide the vector of residuals \mathbf{r} , instead of the scalar χ^2 of [equation \(17\)](#), to compute explicitly the Hessian matrix of the χ^2 merit function. This makes the method much more robust and efficient than generic optimizers of scalar functions.

PPXF uses the state-of-the-art MINPACK implementation of the Levenberg-Marquardt method by [Moré et al. \(1980\)](#), which is based on the robust trust region method. It was converted into IDL and named MPFIT by [Markwardt \(2009\)](#), with the important addition of the ability to set bounds or keep any of the variables fixed. MPFIT was ported to Python by Mark Rivers and later adapted for use with Numpy by Sergey Koposov.

A possible alternative for the non-linear optimization under Python would be the Scipy function `optimize.least_squares`,

introduced in 2016, which is also designed for least-squares problems with bounds and is also based on the trust region method. However, my initial tests indicated it is not yet competitive with MPFIT when used within PPXF.

3.5 Weights regularization for stellar population

To study the star formation history and stellar population of a galaxy, one can model its unobscured, rest-frame spectrum by discretizing the following integral equation (e.g. Cid Fernandes et al. 2005; Tojeiro et al. 2007)

$$G_{\text{mod}}(\lambda) = \int_{t'=0}^{t'=t} \text{SSP}_{\lambda}(t', Z) \cdot \text{SFR}(t - t') dt', \quad (22)$$

where SFR is the star formation rate, SSP_{λ} is a Single Stellar Population spectrum per unit mass, with age t' and metallicity Z , while t is the age of the Universe at the redshift of the galaxy. This expression is straightforwardly generalized in PPXF to study the distribution of more parameters, like e.g. metallicity, α enhancement or IMF, in addition to the SFR (e.g. Conroy 2013, §2.3).

equation (22) is an inhomogeneous Fredholm equation of the first kind, with kernel SSP_{λ} . And the recovery of the $\text{SFR}(t')$ from the observed G_{mod} is a textbook example of ill-conditioned inverse problem (e.g. Press et al. 2007, §19.0). This means that the recovery suffers from severe degeneracies and a unique solution cannot be found without further assumptions.

A standard way of dealing with this type of problem is by using regularization (e.g. Tikhonov & Arsenin 1977; Hansen 1998), which can be thought of as damping the high-frequency variations in the solution, unless they are actually required to describe the data, or finding a trade-off between the quality of the fit and the noise in the solution (e.g. Press et al. 2007, §19.4). In other words, regularization allows one to select the smoothest solution, among the many degenerate solutions that are *equally* consistent with the data.

A conceptual mistake that is often made regarding regularization, is to think that this is equivalent to assuming the solution has to be smooth. This is *not* correct. In fact, the solution can be as non-smooth as required by the data and e.g. it will allow for multiple bursts of star formation if the data require them. The solution will only be smooth if this is consistent with the data.

Under some simplifying assumptions, the regularized solution has a simple Bayesian interpretation: it represents the most likely solution for the weights, given an adjustable prior on the amplitude of the fluctuations (e.g. Press et al. 2007, §19.4.1). An alternative to regularization consists of explicitly exploring the posterior of the allowed solutions using a Markov Chain Monte Carlo approach (e.g. Gilks et al. 1996), while using the individual weights as non-linear model variables. Although potentially interesting and conceptually simple, we found the latter approach quite time consuming for general usage and did not yet include it in PPXF.

Assuming, without loss of generality, that one is performing a spectral fitting study of the stellar population, while varying a single parameter (e.g. age), the smoothness functional is defined as follows (e.g. Press et al. 2007, §19.5)

$$\lambda \mathcal{B} = \lambda \int w''(t)^2 dt \propto \sum_{n=2}^{N-1} \frac{(w_{n-1} - 2w_n + w_{n+1})^2}{\Delta} \quad (23)$$

where the w_n are the spectral weights and the functional is zero only for a linear function of the weights. This expression is straightforwardly extended within PPXF to dimensions large than one, by performing the finite differences separately along every axis. In this

case the software requires the stellar population templates to form a full grid in 2-dim or 3-dim, in such a way that one can easily map the elements of the weights vector onto the 2-dim or 3-dim coordinates in population parameters. A similar regularization approach was used in the STECKMAP full-spectrum fitting code (Ocvirk et al. 2006).

In practice, the regularization is implemented in PPXF by augmenting the matrix equation (19) with one extra row, namely one extra equation, for every term in the summation of equation (23)

$$\frac{w_{n-1} - 2w_n + w_{n+1}}{\Delta} = 0, \quad (24)$$

in such a way that the matrix equation (19) becomes

$$\begin{pmatrix} \mathbf{L}^{-1} \cdot \mathbf{A} \\ \lambda \mathbf{C} \end{pmatrix} \cdot \mathbf{x} = \begin{pmatrix} \mathbf{L}^{-1} \cdot \mathbf{y} \\ 0 \end{pmatrix}, \quad (25)$$

with \mathbf{C} the array with the coefficients of equation (24). This augmented system is still solved by BVLS or NNLS as in the non-regularized case, with the same positivity constraints of equation (18).

3.6 Kinematic bulge disk decomposition

PPXF also includes the possibility to constrain the ratio of the first two kinematic components to a desired value. This can be useful e.g. to perform kinematic bulge-disk decompositions (Tabor et al. in preparation). One can force the template spectra describing the bulge component to contribute a prescribed fraction f_{bulge} of the total flux in the fitted spectrum

$$f_{\text{bulge}} = \frac{\sum w_{\text{bulge}}}{\sum w_{\text{bulge}} + \sum w_{\text{disk}}}, \quad (26)$$

where w_{bulge} and w_{disk} are the weights assigned to the set of spectral templates used to fit the bulge and disk respectively.

This constrain is enforced in the same way as the regularization constraints, by adding the following extra equation to the linear least-squares sub-problem of equation (19)

$$\frac{(f_{\text{bulge}} - 1) \sum w_{\text{bulge}} + f_{\text{bulge}} \sum w_{\text{disk}}}{\Omega} = 0, \quad (27)$$

with the parameter Ω set to a very small number (e.g. $\Omega = 10^{-9}$), which specifies the relative accuracy at which this equation needs to be satisfied. When both the spectral templates and the galaxy spectrum are normalized to have a mean flux of order unity, the best fitting weights w_{bulge} and w_{disk} are generally smaller than unity and equation (27) is satisfied to numerical accuracy.

4 EXTRACTING KINEMATICS AT LOW DISPERSION

In this section I discuss the problem of extracting accurate kinematics using full spectrum fitting, in the special case in which the velocity dispersion is smaller than the velocity step. This is generally chosen to be similar to the instrumental dispersion, to reduce spectral covariance. In what follows I assume the two are the same, and sometimes use them interchangeably, when referring to the critical scale where issues appear.

The problems and solution discussed in this section are illustrated using numerical experiments. My goal is *not* to assess the general ability of PPXF to recover galaxy kinematics, or other practical issues, like the biases as a function of the quality of the stellar templates. This has already been covered in the literature (e.g. Westfall et al. 2011). Instead, I focus here exclusively on the important numerical problems due to the discretization of the LOSVD.

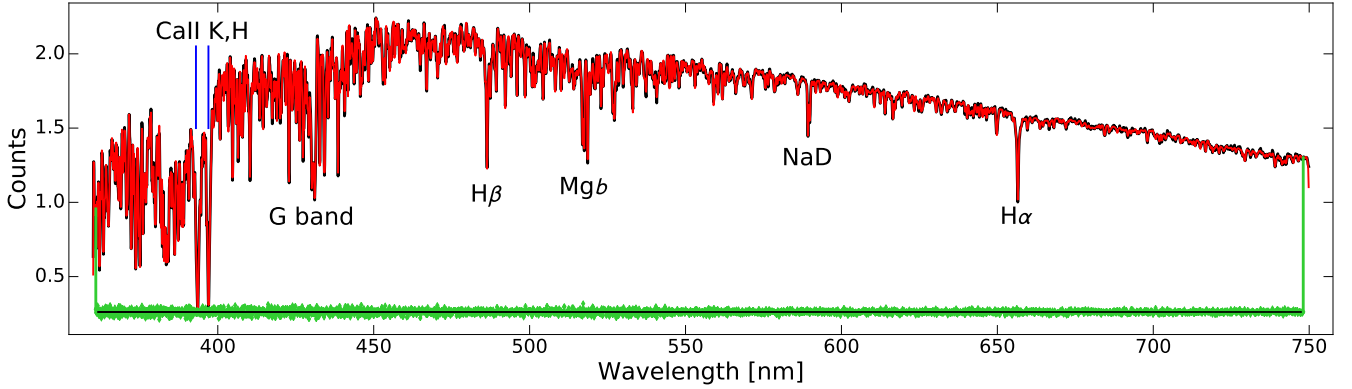


Figure 1. The solar spectrum. The figure illustrates a typical PPXF fit to the solar spectrum by Kurucz (2005) used for our tests. The black line is the relative flux of the observed spectrum (with noise added), for an adopted dispersion $\sigma_{\text{in}} = 140 \text{ km s}^{-1}$, while the red line is the PPXF fit. The green symbols at the bottom are the residuals (arbitrarily offset). The principal absorption features are indicated.

4.1 Setting up the numerical experiments

For the experiments I restrict myself to the wavelength range 360–750 nm, which is a spectral region containing a number of useful absorption features for the kinematic extraction. This wavelength range e.g. is fully covered by the MaNGA (Bundy et al. 2015) and CALIFA (Sánchez et al. 2012) integral-field spectroscopic surveys. This is also the region covered by the spectra of the MILES stellar library (Sánchez-Blázquez et al. 2006). However the results I present are general and are quite insensitive to the adopted wavelength region.

I use as my ‘galaxy’ spectrum the solar spectrum² by Kurucz (2005), which has a resolution $R = \Delta\lambda/\lambda \approx 300\,000$ FWHM and a typical $S/N \approx 3000$ per spectral element. This spectrum can be regarded as having essentially infinite resolution and S/N for all practical purposes of my tests. Also in this case, I have verified that the results of the experiments are general and weakly depend on the specific choice of the input spectrum, as long as it is representative of real high-resolution galaxy spectra. Nearly indistinguishable results were obtained, in all my tests, using e.g. a high-resolution $R = 20\,000$, solar metallicity, 10 Gyr, single stellar population model of Maraston & Strömbäck (2011), based on the MARCS theoretical stellar library (Gustafsson et al. 2008).

I adopt an idealized spectrograph, with a Gaussian LSF, with a constant instrumental dispersion $\sigma_{\text{inst}} = 70 \text{ km s}^{-1}$ (i.e. $R \approx 1800$ FWHM). This is the median resolution of the MaNGA spectrograph, but is also similar to the one used by other galaxy surveys: it is similar to the low-resolution mode used by the SAMI survey (Bryant et al. 2015), the high-resolution mode used by the CALIFA survey (Sánchez et al. 2012), or the resolution of the ATLAS^{3D} survey (Cappellari et al. 2011). I assume the spectra are Nyquist sampled by the detector, and consequently adopt a spectral pixel $(\Delta x)_{\text{pixel}} = \sigma_{\text{inst}} = 70 \text{ km s}^{-1}$. This is the same velocity sampling adopted e.g. by the SDSS data release 12 (Alam et al. 2015).

I investigate the case where I use as input stellar template in PPXF the same spectrum used for the galaxy spectrum. I further assume a quite high $S/N = 200$ per spectral interval $(\Delta x)_{\text{pixel}}$. Both choices are made again to provide a clean experiment which isolates the under-sampling problem from e.g. the unrelated issue of template mismatch. I adopt the default degree=4 additive polyno-

mials, but my results are totally insensitive to this choice. A representative PPXF fit to the solar spectrum is shown in Figure 1.

In my experiments, the solar spectrum was initially logarithmically sampled with velocity scale of 2 km s^{-1} per pixel, which is an integer factor smaller than the final detector pixels. Subsequently, the spectrum was accurately convolved with a very well-sampled, discretized LOSVD and with a Gaussian LSF. Then the spectrum was integrated over the 70 km s^{-1} wide pixels, by summing every adjacent set of 35 pixels. Finally noise was added to every pixel. In the tests, the input velocity was chosen randomly for every realization, to prevent the LOSVD from being aligned in a constant manner with respect to the pixels boundaries. The same applies to the starting guess for V and σ , which were chosen randomly for every realization.

I emphasize the fact that for the initial LOSVD convolution I did *not* use the analytic Fourier transform introduced in this paper. This provides a useful debugging of my implementation. In fact a good recovery can only be achieved if the analytic Fourier approach correctly corresponds to the discrete version, in the limit of a well-sampled kernel, and when the spectrum contains information on the Gauss-Hermite coefficients, namely when $\sigma \gtrsim \sigma_{\text{inst}}$.

4.2 Description of the problem

The convolution of the templates with the broadening function in equation (11) is performed by PPXF according to the discrete definition

$$(T * \mathcal{L})_p \equiv \sum_{q=-Q/2}^{Q/2} T_{q+p} \mathcal{L}_q, \quad (28)$$

where Q is the number of elements where the kernel $\mathcal{L}_q \equiv \mathcal{L}(cx_q)$ is non-zero and $T_q \equiv T(x_q)$. In practice, for computational efficiency, this convolution is performed using the standard Fourier approach (e.g. Press et al. 2007, §13.1)

$$T * \mathcal{L} = \mathcal{F}^{-1} [\mathcal{F}(T) \cdot \mathcal{F}(\mathcal{L})] \quad (29)$$

where \mathcal{F} is the Discrete Fourier Transform (DFT) and \mathcal{F}^{-1} is its inverse, which can be computed efficiently with a number of operations proportional to $P \log P$ using the classic Fast Fourier Transform (FFT) algorithm (Cooley & Tukey 1965). For efficiency, PPXF pre-computes the $\mathcal{F}(T)$ of all the templates, as this does not

² Available from <http://kurucz.harvard.edu/sun/>

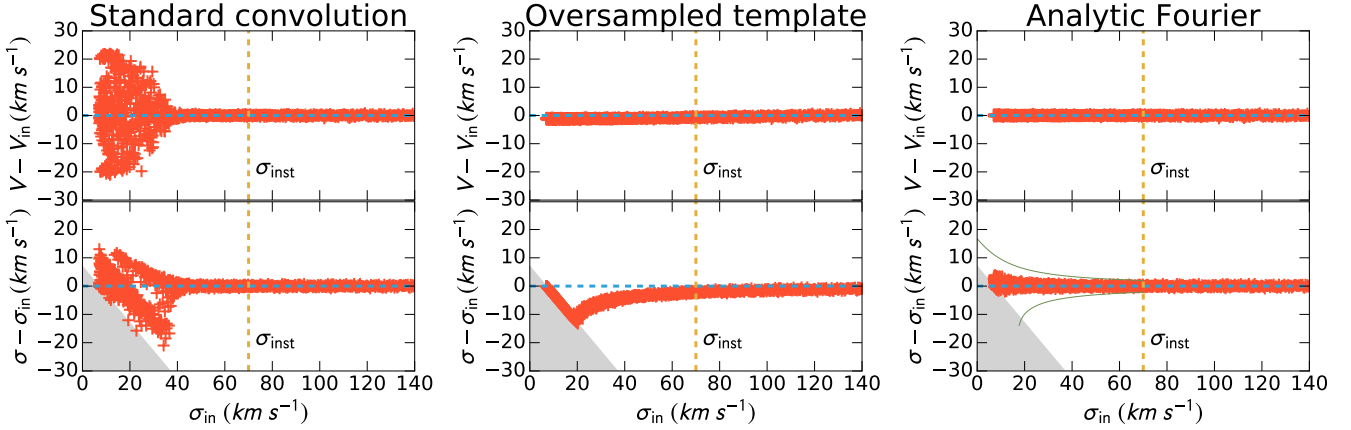


Figure 2. Kinematics recovery with a Gaussian LOSVD. The three panels illustrate the ppxf recovery of the velocity V and dispersion σ for an adopted Gaussian LOSVD with known velocity V_{in} and dispersion σ_{in} . The grey area indicates the region of $\sigma < \sigma_{\text{inst}}/10$, which is not allowed by the program. The vertical dashed line indicates the instrumental dispersion $\sigma_{\text{inst}} = 70 \text{ km s}^{-1}$, which coincides with the adopted velocity sampling $(\Delta x)_{\text{pix}}$. *Left Panel:* recovery without oversampling. Note the dramatic increase of the errors below $\sigma_{\text{in}} \lesssim \sigma_{\text{inst}}/2$. *Middle Panel:* recovery with oversampling of both the LOSVD and the template by a factor of 10. This approach is slower and produces a significant drop in the dispersion below $\sigma_{\text{in}} \lesssim \sigma_{\text{inst}}/2$. *Right Panel:* recovery with the solution proposed in this paper, namely using an analytic Fourier transform of the LOSVD. This is at least as fast as the left panel, but here both V and σ are recovered without bias.

changes during the χ^2 minimization, and uses the specific FFT for real input, NumPy's `fft.rfft` based on FFTPACK (Swarztrauber 1982), which further decrease the FFT computation time by a factor of two.

For the discrete convolution, the LOSVD, which acts as convolution kernel, is sampled at discrete intervals $(\Delta x)_{\text{pixel}} = (\Delta v)_{\text{pixel}}/c$ before the computation of $\mathcal{F}(\mathcal{L})$. This straightforward approach of discretely sampling the kernel, represents the standard practice, when one needs to perform convolutions of spectra or images with Gaussian kernels. It is used e.g. in the `GAUSS.SMOOTH` function in IDL, in the `ndimage.filters.gaussian_filter` function of the Python package Scipy, or in the `convolution.Gaussian1DKernel` function of the Python package ASTROPY.

However, it is clear that, when $\sigma \lesssim (\Delta x)_{\text{pixel}}$, where σ is the dispersion of the Gaussian, the kernel starts becoming severely under-sampled and cannot be expected to accurately represent the LOSVD any more. As an illustration, when the Gaussian is centred on a pixel and $\sigma = (\Delta x)_{\text{pixel}}/2$, the kernel has essentially only three non-zero elements $\mathcal{L} = (0.14, 1, 0.14)$, fully dominated by the middle one.

One should not expect a reliable recovery of the LOSVD at these low dispersion, and in particular, both the velocity and the dispersion should not be expected to be determined to better than about half a pixel. This was the reason why ppxf included the `oversample` keyword to oversample both the LOSVD and the template before the calculation of $\mathcal{F}(T)$ and $\mathcal{F}(\mathcal{L})$. This approach however suffer from two limitations: (i) it requires a significant increase in the size of the template spectra, resulting in an increase of the computation time and (ii) the oversampling of the templates is smooth below the observed scale, and does not represent the dense forest of thin absorption lines in real stellar spectra.

The left panel of Figure 2 illustrates the dramatic problems which appear when $\sigma_{\text{in}} \lesssim (\Delta x)_{\text{pixel}}/2$, while adopting a Gaussian input LOSVD: ppxf becomes essentially unable to reliably recover both the velocity and the dispersion of the LOSVD. In fact, although the velocity has an rms error of only 0.3 km s^{-1} , when

$\sigma_{\text{in}} > (\Delta x)_{\text{pixel}}$, the errors become as high as 20 km s^{-1} at low σ_{in} . This problem is not specific to ppxf but will affect any spectral fitting program that uses the standard equation (28) to define convolution.

The middle panel of Figure 2 shows that, as expected, by oversampling both the LOSVD and the template, the velocity can be well recovered, however the dispersion tends to be under-estimated at low σ_{in} , because the oversampled template is smoother than the real spectrum.

Similar problems can be seen when the LOSVD is assumed to be described by a significantly non-Gaussian shape, parametrized by equation (13). I adopted as input some realistic values $h_3 = h_4 = 0.1$ (e.g. Emsellem et al. 2004). Note that, contrary to what we did in Cappellari & Emsellem (2004), here I assume the input LOSVD to be precisely described by the adopted parametrization, because I want to test the precise recovery of the *known* input Gauss-Hermite moments.

The left panel of Figure 3 again illustrates the dramatic problems in the recovery of the velocity and dispersion, when $\sigma_{\text{in}} \lesssim (\Delta x)_{\text{pixel}}/2$. In this case, with non-Gaussian LOSVD, one can see the expected convergence towards zero of the h_3 and h_4 parameters, due to the penalty term in equation (21). For all the examples in Figure 3 I adopted the same penalty `bias=1` in ppxf. This becomes important for $\sigma_{\text{in}} \lesssim (\Delta x)_{\text{pixel}}/2$, where the broadening by the instrumental dispersion makes the deviations from a Gaussian hard to measure and ppxf tries to penalize the LOSVD towards a Gaussian. But at the smallest σ_{in} even the penalty loses its effectiveness, and one can see sharp variations, especially in the recovered h_4 , instead of the desired convergence toward zero (i.e. Gaussian shape).

The middle panel of Figure 3 again shows that by oversampling the LOSVD and the template one can overcome the main problems with the recovery of the velocity. However the velocity dispersion shows the same behaviour as in the middle panel of Figure 2, with the recovered σ being severely underestimated, and hitting the lower boundary, when $\sigma_{\text{in}} \lesssim 20 \text{ km s}^{-1}$.

4.3 Solution of the problem

A solution to the under-sampling problem comes by noting that the Fourier transform of the kernel happens to be analytic in the special case of interest, where the LOSVD is parametrized by the Gauss-Hermite series of [equation \(13\)](#). This suggests one can use an analytic rather than discrete Fourier transform to evaluate $\mathcal{F}(\mathcal{L})$ in [equation \(29\)](#).

If I define the continuous Fourier transform of a time-domain function $h(t)$, using the modern-physics convention, with ω the angular frequency, as

$$H(\omega) = \frac{1}{\sqrt{2\pi}} \int_{-\infty}^{\infty} h(t) e^{i\omega t} dt, \quad (30)$$

the $H(\omega)$ of the LOSVD has an exceedingly simple form. This is because the individual terms of \mathcal{L} are eigenfunction of the $H(\omega)$ operator. This fact was already pointed out by [van der Marel & Franx \(1993, eq. A7\)](#) and of course can be verified analytically. It is a textbook result (e.g. [Schiff 1968, §4](#)), related to the fact that the terms of [equation \(13\)](#) are the wavefunctions of the quantum harmonic oscillator. These have the same form in either position or momentum-space, which are related via the Fourier transform. Specifically, if one defines

$$\mathcal{L}_m(t) = \frac{\exp(-t^2/2)}{\sigma\sqrt{2\pi}} H_m(t) \quad (31)$$

the following simple transform pair holds

$$h(t) = \mathcal{L}_m(t) \iff H(\omega) = i^m \mathcal{L}_m(\omega). \quad (32)$$

In other words, the $H(\omega)$ have the same form as the original \mathcal{L}_m functions, simply transformed into the frequency domain, while the even/odd terms are alternating real/imaginary respectively. This latter fact comes from two general properties of $H(\omega)$: (i) if $h(t)$ is real and even, then the same is true for $H(\omega)$; (ii) if $h(t)$ is real and odd, then $H(\omega)$ is imaginary and odd.

The analytic calculation of $\mathcal{F}(\mathcal{L})$ has two major advantages, with respect to its discrete version. They derive from general properties of the Fourier Transform (e.g. [Brigham 1974, §3](#)):

Good kernel sampling: When the LOSVD is narrow, and consequently poorly sampled, in the ‘time’ or spatial domain, it will become broad in the frequency domain according to the transform pair

$$\frac{1}{|\sigma|} h\left(\frac{t}{\sigma}\right) \iff H(\sigma\omega) \quad \text{frequency scaling.} \quad (33)$$

This implies that the LOSVD will never be under-sampled in the frequency domain because it is necessarily non-zero only for a small fraction of the size of the full template spectrum.

Simple velocity shifting: When evaluating the kernel of [equation \(13\)](#) for the discrete convolution of [equation \(28\)](#), one needed to sample a symmetric range of velocities from $-v_{\max}$ to v_{\max} , fully enclosing the offset LOSVD. This produced many zero elements in the kernel, causing practical issues with large V . In Fourier space this problem disappears as one can use

$$h(t - t_0) \iff H(\omega) e^{i\omega t_0} \quad \text{time shifting} \quad (34)$$

to shift the velocity of the templates by simply changing the phase of all elements of the complex transform.

4.4 Final formula and tests

Combining [equation \(32\)](#) to [equation \(34\)](#), I find that the analytic Fourier transform of the LOSVD of [equation \(13\)](#) is

$$H(\omega) = \frac{\exp(i\omega V - \sigma^2\omega^2/2)}{\sqrt{2\pi}} \left[1 + \sum_{m=3}^M i^m h_m H_m(\sigma\omega) \right]. \quad (35)$$

This expression is used to compute the DFT $\mathcal{F}(\mathcal{L})$ which appears in [equation \(29\)](#). Given that \mathcal{L} is a real function, it is uniquely defined over half of the frequencies

$$h(t) \text{ is real} \implies H(-\omega) = [H(\omega)]^*. \quad (36)$$

This implies that one only needs to evaluate $H(\omega)$ of [equation \(35\)](#) in the interval $\omega = [0, \pi]$ to obtain the DFT of real input. This needs to have the same number of elements as the DFT of real input $\mathcal{F}(T)$, namely half the size of T .

The right panel of [Figure 2](#) illustrates the dramatic improvement in the recovery of both the velocity and the dispersion, when using the analytic Fourier transform approach. No biases can be detected in the recovery, and importantly, the scatter in the recovered values is nearly independent of σ_{in} . The trend in velocity is similar to that with the overampled template, however the small trend (due to unclear reasons, but related to the adopted interpolation) completely disappear. The σ is recovered without detectable bias, and in particular, the underestimation of σ that affects the oversampled case, also disappears.

Similar conclusions apply to the case with non-Gaussian LOSVD in the right panel of [Figure 3](#). Also in this case, PPXF using the analytic $\mathcal{F}(\mathcal{L})$ looks similar to the oversampled case, but now the σ underestimation disappears. Note that the penalty of PPXF is still important to prevent wildly degenerate solutions and consequently large noise in all parameters when $\sigma_{\text{in}} \lesssim (\Delta x)_{\text{pixel}}$. This important aspect was described in detail in [Cappellari & Emsellem \(2004\)](#). It is still relevant here, but the discussion will not be repeated.

In the right panel of [Figure 3](#), are also shown, with thin lines, the variations in the recovered σ one should expect when the assumed instrumental dispersion is in error by a $\sigma_{\text{inst}} = \pm 3\%$. This is not an unrealistic uncertainty, but instead represents an optimistic estimate in realistic conditions, for the combined uncertainties in σ_{diff} in [equation \(5\)](#). The curves illustrate the fact that, at $\sigma \lesssim (\Delta x)_{\text{pixel}}/2$, biases in σ will be dominated by the uncertainty in the LSF.

If stellar templates are available with higher resolution than the galaxy, it makes sense to avoid the degradation of the templates to the galaxy resolution. For this reason PPXF was modified to allow input templates with a smaller velocity scale than the galaxy. It is also possible to skip the broadening of the templates to the galaxy LSF described in [subsection 2.2](#) and instead include the Gaussian convolution in [equation \(35\)](#) for $H(\omega)$, using the associative property of the convolution. An additional convolution by a Gaussian is obtained by multiplying $H(\omega)$ by the Gaussian Fourier transform. This implies that a convolution with the Gaussian of [equation \(4\)](#) is obtained by replacing the term inside the exponential in [equation \(35\)](#) with

$$i\omega V - (\sigma_{\text{diff}}^2 + \sigma^2)\omega^2/2. \quad (37)$$

To use this expression σ_{diff} must be constant in km s^{-1} . This must be achieved by homogenizing the template resolution in such a way that it has a constant σ_{diff} .

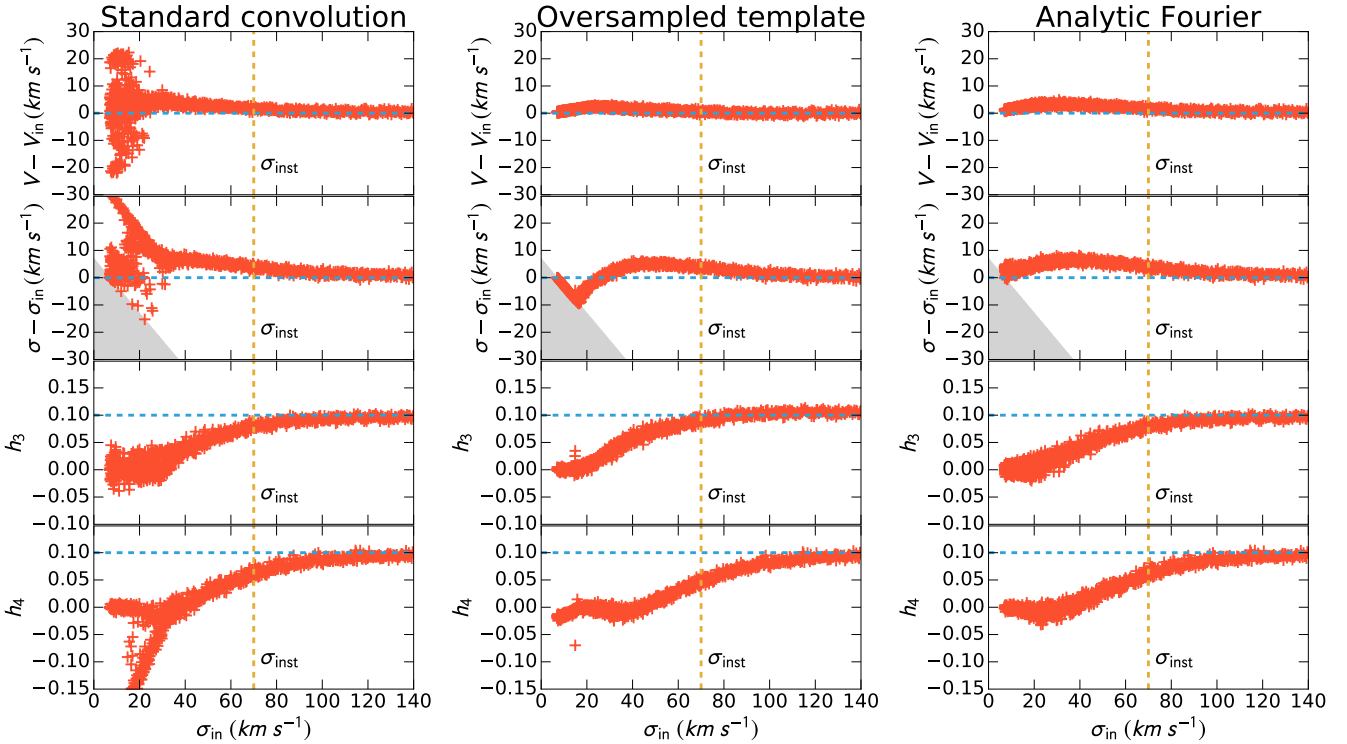


Figure 3. Kinematics recovery with a LOSVD described by the Gauss-Hermite parametrization. The three panels illustrate the PPXF recovery of the kinematics for a LOSVD with adopted velocity V_{in} , dispersion σ_{in} and realistic $h_3 = h_4$. The grey area indicates the region of $\sigma < \sigma_{\text{inst}}/10$, which is not allowed by the program. The vertical dashed line indicates the instrumental dispersion $\sigma_{\text{inst}} = 70 \text{ km s}^{-1}$, which coincides with the adopted velocity sampling $(\Delta x)_{\text{pix}}$. *Left Panel:* recovery without oversampling. Note the dramatic increase of the errors below $\sigma_{\text{in}} \lesssim \sigma_{\text{inst}}/2$. *Middle Panel:* recovery with oversampling of both the LOSVD and the template by a factor of 10. This approach is slower and produces a significant drop in the dispersion below $\sigma_{\text{in}} \lesssim \sigma_{\text{inst}}/2$. *Right Panel:* recovery with the solution proposed in this paper, namely using an analytic Fourier transform of the LOSVD. This is at least as fast as the left panel, but here all kinematics parameters are properly recovered. Note that h_3 and h_4 start converging towards zero (i.e. Gaussian LOSVD) when $\sigma_{\text{in}} \lesssim \sigma_{\text{inst}}$. This is intentional and unavoidable. It is used to prevent a dramatic increase of the errors in V and σ when the parameters of the LOSVD become degenerate at low σ_{in} . This effect is extensively discussed in Cappellari & Emsellem (2004).

4.5 Relation to previous work

I have not found previous usage in the literature of an analytic Fourier transform to improve the accuracy of the spectral fitting method. However the general idea is obviously a good one and for this reason it was used before in the literature, in a similar context, for the special case of Gaussian functions.

An analytic Fourier transform was used for the kinematic extraction from galaxy spectra, when using Fourier methods, where the advantage of this approach is more apparent than in pixels space. For example, the usage of an analytic Fourier transform of a Gaussian broadening function was described by Sargent et al. (1977); Schechter & Gunn (1979) for their improved version of the Fourier quotient method. The analytic transform was fitted in Fourier space to the ratio of the FFT of the galaxy and template. An analytic Fourier transform of the Gaussian was also used by Tonry & Davis (1979) in their analysis of the errors of the cross-correlation method.

I found applications of an analytic Fourier transform for convolution in image processing. For example, the algorithm I describe in subsection 4.4 for the Gauss-Hermite functions is a generalization of the algorithm 5 in the survey of Gaussian convolution algorithms by Getreuer (2013). In that paper, the author also discusses the discretization aspects, namely the meaning of combining a DFT with an analytic Fourier transform, sampled at discrete intervals. I

ignored that aspect here, but instead tested numerically that the approach recovers the known input with the desired accuracy.

5 SUMMARY

In the first part of the paper, I provided an overview, or tutorial, of general concepts useful to understand and properly interpret the extraction of kinematics from galaxy spectra. I tried to clarify in particular the questions I received more often, over more than a decade, from users of my publicly available PPXF software.

Then I gave an updated overview of the PPXF method. I focused especially on the description of features of the method which had been included after the publication of the original paper, some of which had never been properly explained and precisely documented in the literature.

Subsequently, I focused on the problem of extracting kinematics via full spectrum fitting, when the velocity dispersion is smaller than the spectral sampling, which is generally chosen to be the same as the instrumental dispersion, to limit spectral covariance. I illustrated the obvious but dramatic problems that arise when one completely ignores the issue, as well as the limitations of the previous solution, which consist of oversampling the spectra.

Finally I provided a clean solution to the long-standing under-sampling issue, which consist of using the analytic Fourier trans-

form of the LOSVD in conjunction with the convolution theorem. This approach completely removes the need for oversampling and makes the full spectrum fitting method suitable for measuring reliable kinematics at any velocity dispersion. This is especially crucial for the mean velocity, which now becomes a well-determined quantity even when the dispersion becomes negligible, and consequently impossible to reliably recover from real data.

The approach described in this paper was implemented in a significant revision to the publicly available code `PRXF`, and is already being used as part of the MaNGA Data Analysis Pipeline (Wesfall et al. in preparation). Further tests on real IFS data will be published elsewhere.

The proposed solution appears quite natural, however, perhaps surprisingly, it is currently not being used by any of the popular software packages. Given the simplicity of our approach for accurate convolutions, we argue it should become standard practice.

ACKNOWLEDGEMENTS

This paper was motivated by productive discussions within the MaNGA Data Analysis Pipeline team and in particular with Kyle Wesfall and Matt Bershad. I thank Samantha Penny for starting the discussion on this subject. I am also grateful to Eric Emsellem and Daniel Thomas for comments. I acknowledge support from a Royal Society University Research Fellowship. This paper made use of matplotlib (Hunter 2007).

REFERENCES

- Abramowitz M., Stegun I. A., 1964, *Handbook of Mathematical Functions* (Reprinted 1972). National Bureau of Standards, Washington
- Alam S., et al., 2015, *ApJS*, **219**, 12
- Alatalo K., et al., 2011, *ApJ*, **735**, 88
- Barrera-Ballesteros J. K., et al., 2015, *A&A*, **582**, A21
- Bender R., Saglia R. P., Gerhard O. E., 1994, *MNRAS*, **269**, 785
- Bershad M. A., Verheijen M. A. W., Swaters R. A., Andersen D. R., Westfall K. B., Martinsson T., 2010, *ApJ*, **716**, 198
- Brigham O. E., 1974, *The fast Fourier transform*. Prentice-Hall Inc., Englewood Cliffs, NJ
- Bruzual G., Charlot S., 2003, *MNRAS*, **344**, 1000
- Bryant J. J., et al., 2015, *MNRAS*, **447**, 2857
- Bundy K., et al., 2015, *ApJ*, **798**, 7
- Calzetti D., Armus L., Bohlin R. C., Kinney A. L., Koornneef J., Storchi-Bergmann T., 2000, *ApJ*, **533**, 682
- Cappellari M., 2016, *ARA&A*, **54**, in press (arXiv:1602.04267)
- Cappellari M., Emsellem E., 2004, *PASP*, **116**, 138
- Cappellari M., et al., 2009, *ApJ*, **704**, L34
- Cappellari M., et al., 2011, *MNRAS*, **413**, 813
- Cappellari M., et al., 2012, *Nature*, **484**, 485
- Cappellari M., et al., 2013a, *MNRAS*, **432**, 1709
- Cappellari M., et al., 2013b, *MNRAS*, **432**, 1862
- Cappellari M., et al., 2015, *ApJ*, **804**, L21
- Cardelli J. A., Clayton G. C., Mathis J. S., 1989, *ApJ*, **345**, 245
- Cenarro A. J., Cardiel N., Gorgas J., Peletier R. F., Vazdekis A., Prada F., 2001, *MNRAS*, **326**, 959
- Cheung E., et al., 2016, *Nature*, **533**, 504
- Cid Fernandes R., Mateus A., Sodré L., Stasińska G., Gomes J. M., 2005, *MNRAS*, **358**, 363
- Conroy C., 2013, *ARA&A*, **51**, 393
- Conroy C., van Dokkum P., 2012, *ApJ*, **747**, 69
- Cooley J. W., Tukey J. W., 1965, *Mathematics of computation*, **19**, 297
- Davis T. A., et al., 2011, *MNRAS*, **417**, 882
- Emsellem E., et al., 2004, *MNRAS*, **352**, 721
- Emsellem E., et al., 2011, *MNRAS*, **414**, 888
- Gerhard O. E., 1993, *MNRAS*, **265**, 213
- Getreuer P., 2013, *Image Processing On Line*, 2013, 286
- Gilks W., Richardson S., Spiegelhalter D., 1996, *Markov chain Monte Carlo in practice*. Chapman & Hall/CRC, Boca Raton
- Gustafsson B., Edvardsson B., Eriksson K., Jørgensen U. G., Nordlund Å., Plez B., 2008, *A&A*, **486**, 951
- Hansen P. C., 1998, *Rank-deficient and discrete ill-posed problems: numerical aspects of linear inversion*. Mathematical Modeling and Computation Vol. 4, Siam, Philadelphia, doi:10.1137/1.9780898719697
- Ho I.-T., et al., 2016, *MNRAS*, **457**, 1257
- Hogg D. W., 1999, arXiv, pp e-print (astro-ph/9905116)
- Hunter J. D., 2007, *Computing In Science & Engineering*, **9**, 90
- Johnston E. J., Merrifield M. R., Aragón-Salamanca A., Cappellari M., 2013, *MNRAS*, **428**, 1296
- Kelson D. D., Illingworth G. D., van Dokkum P. G., Franx M., 2000, *ApJ*, **531**, 159
- Krajnović D., Cappellari M., de Zeeuw P. T., Copin Y., 2006, *MNRAS*, **366**, 787
- Krajnović D., McDermid R. M., Cappellari M., Davies R. L., 2009, *MNRAS*, **399**, 1839
- Kurucz R. L., 2005, *Memorie della Societa Astronomica Italiana Supplementi*, **8**, 189
- Lawson C. L., Hanson R. J., 1974, *Solving least squares problems* (SIAM 1995 edition). Classics in applied mathematics Vol. 15, Prentice-Hall Inc., Englewood Cliffs, NJ, doi:10.1137/1.9781611971217
- Maraston C., Strömbäck G., 2011, *MNRAS*, **418**, 2785
- Markwardt C. B., 2009, in D. A. Bohlender D. Durand . P. D., ed., *Astronomical Society of the Pacific Conference Series Vol. 411, Astronomical Data Analysis Software and Systems XVIII*. p. 251 (arXiv:0902.2850)
- McDermid R. M., et al., 2015, *MNRAS*, **448**, 3484
- More J., Garbow B., Hillstom K., 1980, *User guide for MINPACK-1*. Argonne National Laboratory Argonne, IL
- Morelli L., Corsini E. M., Pizzella A., Dalla Bontà E., Coccato L., Méndez-Abreu J., 2015, *MNRAS*, **452**, 1128
- Munari U., Sordo R., Castelli F., Zwitter T., 2005, *A&A*, **442**, 1127
- Naab T., et al., 2014, *MNRAS*, **444**, 3357
- Ocvirk P., Pichon C., Lançon A., Thiébaud E., 2006, *MNRAS*, **365**, 74
- Onodera M., et al., 2012, *ApJ*, **755**, 26
- Press W. H., Teukolsky S. A., Vetterling W. T., Flannery B. P., 2007, *Numerical recipes: The art of scientific computing*, 3rd edn. Cambridge Univ. Press, Cambridge
- Prugniel P., Soubiran C., 2001, *A&A*, **369**, 1048
- Rix H.-W., White S. D. M., 1992, *MNRAS*, **254**, 389
- Sánchez-Blázquez P., et al., 2006, *MNRAS*, **371**, 703
- Sánchez S. F., et al., 2012, *A&A*, **538**, A8
- Sargent W. L. W., Schechter P. L., Boksenberg A., Shorridge K., 1977, *ApJ*, **212**, 326
- Sarzi M., Falcón-Barroso J., Davies R. L., et al. 2006, *MNRAS*, **366**, 1151
- Schechter P. L., Gunn J. E., 1979, *ApJ*, **229**, 472
- Schiff L. I., 1968, *Quantum Mechanics* 3rd ed.. McGraw-Hill, New York
- Scott N., et al., 2015, *MNRAS*, **451**, 2723
- Seth A. C., et al., 2014, *Nature*, **513**, 398
- Shetty S., Cappellari M., 2015, *MNRAS*, **454**, 1332
- Swartztrauber P. N., 1982, in Rodrigue G., ed., *Parallel Computations*. Academic Press, New York, pp 51–83, doi:10.1016/B978-0-12-592101-5.50007-5
- Tikhonov A. N., Arsenin V. Y., 1977, *Solutions of ill-posed problems*. Wiley, New York
- Tojeiro R., Heavens A. F., Jimenez R., Panter B., 2007, *MNRAS*, **381**, 1252
- Tonry J., Davis M., 1979, *AJ*, **84**, 1511
- Vazdekis A., Sánchez-Blázquez P., Falcón-Barroso J., Cenarro A. J., Beasley M. A., Cardiel N., Gorgas J., Peletier R. F., 2010, *MNRAS*, **404**, 1639
- Walsh J. L., van den Bosch R. C. E., Gebhardt K., Yıldırım A., Richstone D. O., Gültekin K., Husemann B., 2016, *ApJ*, **817**, 2
- Weijmans A.-M., et al., 2009, *MNRAS*, **398**, 561

- Westfall K. B., Bershady M. A., Verheijen M. A. W., 2011, [ApJS](#), **193**, 21
- de Zeeuw P. T., et al., 2002, [MNRAS](#), **329**, 513
- van der Marel R. P., 1994, [MNRAS](#), **270**, 271
- van der Marel R. P., Franx M., 1993, [ApJ](#), **407**, 525
- van der Marel R. P., Rix H. W., Carter D., Franx M., White S. D. M., de Zeeuw T., 1994, [MNRAS](#), **268**, 521